

Examining the influence of anisotropy on the fundamental mode of nonradial oscillation in neutron stars on a complete general relativistic scheme

José D. V. Arbañil^{a,b,1} Gabriel O. Cavalleiro^c Victor B. T. Alves^d Juan M. Z. Pretel^e César O. V. Flores^{d,f} César H. Lenzi^c

^aDepartamento de Ciencias, Universidad Privada del Norte,
Avenida el Sol 461 San Juan de Lurigancho, 15434 Lima, Peru.

^bFacultad de Ciencias Físicas, Universidad Nacional Mayor de San Marcos,
Avenida Venezuela s/n Cercado de Lima, 15081 Lima, Peru.

^cDepartamento de Física, Instituto Tecnológico de Aeronáutica,
São José dos Campos, São Paulo, CEP 12228-900, Brazil.

^dPrograma de Pós-graduação em Física, Universidade Federal do Maranhão, São Luís, Maranhão, CEP 65080-805, Brazil.

^eCentro Brasileiro de Pesquisas Físicas,
Rua Dr. Xavier Sigaud, 150 URCA, Rio de Janeiro CEP 22290-180, RJ, Brazil.

^fUniversidade Estadual da Região Tocantina do Maranhão,
Centro de Ciências Exatas, Naturais e Tecnológicas, Imperatriz, Maranhão, CEP 65901-480, Brazil.

E-mail: jose.arbanil@upn.pe, gabrieloliveira8551@gmail.com,
victor.bruno@discente.ufma.br, juanzarate@cbpf.br,
cesar.vasquez@uemasul.edu.br, chlenzi@ita.br

Abstract. The anisotropic influence on the f -mode frequency of oscillations and dimensionless tidal deformability of neutron stars are analyzed by employing the nonradial oscillation equations for the complete general relativity frame and tidal deformability equations, which are derived and modified from their standard form to introduce the anisotropic factor. The fluid inside the compact star obeys an equation of state constructed by matching microscopic nuclear and perturbative QCD calculations through a piecewise polytropic interpolating scheme. For the anisotropic function, we use a local anisotropy, which is regular along the whole star and is null both at the center and on the star's surface. We show that the f -frequency of oscillation and dimensionless tidal deformability change considerably with the anisotropy. Finally, we investigate the correlation between the dimensionless tidal deformability of the GW170817 event with the anisotropy.

¹Corresponding author.

Contents

1	Introduction	1
2	General relativistic equations	3
2.1	The static equilibrium equations	3
2.2	Nonradial perturbation equations	4
2.3	Tidal deformability	6
3	Equation of state and anisotropic profile	7
3.1	Equation of state	7
3.2	Anisotropic profile	8
4	Anisotropic effects on the equilibrium, frequency of oscillations, and tidal deformability	9
4.1	General remarks	9
4.2	Equilibrium configurations and frequency of oscillations	10
4.3	On the detectability of the fundamental mode signal	12
4.4	Tidal deformability	13
5	Conclusions	15
A	Nonradial perturbations of relativistic spherically symmetric stars in the presence of an anisotropic fluid	16
A.1	Perturbative variables	16
A.2	Perturbation equations	17
B	Perturbation functions near $r = 0$	19

1 Introduction

Since the first detection of gravitational wave (GW) signals from a binary neutron star (NS) merger, known as GW170817 and reported by the LIGO-Virgo Collaboration (LVC) [1], numerous researchers have made significant efforts to explore the microphysics of NSs in more depth, providing stringent constraints on the equation of state (EOS) of such stars and significantly narrowing the range of possible theoretical models. In other words, the GW analysis provides a promising avenue for probing the behavior of ultra-dense matter under extreme conditions. This can be achieved by studying the EOS through the gravitational waves generated during the merger of two compact stars. Nevertheless, the GW170817 event is only one of the many and varied multi-messenger sources that can be observed using ground-based GW detectors [2–9]. Furthermore, future space-based GW observatories like DECIGO are expected to open a new window for probing new physics related to highly deformed compact objects, such as NSs, hybrid stars, and magnetars, which are currently inaccessible to ground-based detectors [10].

Asteroseismology is a powerful theoretical tool for gaining a deeper understanding of the behavior of dense matter inside compact stars [11–14]. Numerous studies have explored pulsation modes assuming various compositions of the isotropic fluid within compact stars,

including deconfined quark matter [15], color-flavor-locked strange quark matter [16], hadronic matter [17, 18], scenarios with density discontinuities [19], and hadronic matter admixed with dark matter [20], among others. These studies consistently show that nonradial oscillation modes are highly sensitive to the microphysical characteristics of the fluid within compact stars, leading to significant variations in their behavior. It is also worth mentioning that third-generation instruments are expected to be more sensitive to continuous GW signals from, e.g., r -mode or f -mode instabilities, from NS mountains [21, 22] or due to resonances in compact binary systems [23].

One of the most widely accepted assumptions in the study of compact stars is that the dense fluid within these objects is isotropic. Nonetheless, theoretical evidence suggests that various phenomena may induce anisotropy in fluids under extreme conditions [24–26], see also the review articles [27, 28] for extensive discussions on anisotropic pressure in self-gravitating systems. In addition, it has been shown in recent years that the inclusion of anisotropy in relativistic star systems leads to theoretical predictions that are consistent with several observational mass-radius measurements and tidal deformability constraints [29–32]. Motivated by these studies, in the present work, we investigate the impact of anisotropic pressure on the f -mode (fundamental mode) oscillation frequency and tidal deformability of neutron stars by using an equation of state obtained by consistently matching microscopic nuclear calculations with perturbative Quantum Chromodynamics (QCD) results, connected through a piecewise polytropic interpolation framework. For this purpose, we derive the nonradial oscillation equations and the regularity conditions for the perturbation variables near the center within the framework of general relativity for anisotropic matter. These equations, together with the deformability equations, are then integrated to assess the influence of anisotropy on the fundamental oscillation modes and stellar deformability.

It is worth noting that, in a similar context, the impact of anisotropy on quasinormal modes of neutron stars [33, 34] and on the fundamental oscillation modes of neutron stars [35, 36] and quark stars [37] has already been investigated. The nonradial oscillation equations derived in this study are consistent with those reported in [33–35], but differ from the expressions presented in [36, 37]. The difference with the last two studies occurs because, in the anisotropic case, the first law of thermodynamics needs to consider that the work done on the fluid varies with direction.

This manuscript is structured as follows: Section 2 presents the hydrostatic equilibrium equations and the nonradial oscillations equations, including the anisotropic factor. Section 3 shows the EOS and the anisotropic profile equation, and in Section 4 we report the results in the analysis of effects of the anisotropy on the equilibrium, frequency of oscillations, and tidal deformability. In Section 5, we conclude. Finally, in Appendix A, the perturbation variables and the general form of the linearized perturbation equations for the anisotropic case are presented. In Appendix B, the perturbation functions explicitly expanded at the star center are presented, which are important to guarantee finite and numerically stable solutions. Throughout this article, we adopt geometric units by setting $G = 1 = c$ to simplify the equations and facilitate numerical calculations.

2 General relativistic equations

2.1 The static equilibrium equations

For completeness, we start by writing the Einstein field equation in the presence of anisotropic matter:

$$G_{\mu\nu} = 8\pi T_{\mu\nu}, \quad (2.1)$$

with the Greek indices μ, ν , etc., run from 0 to 3. $G_{\mu\nu}$ represents the Einstein tensor and $T_{\mu\nu}$ stands the stress-energy tensor that is given by:

$$T_{\mu\nu} = (p_r + \sigma) g_{\mu\nu} + (\rho + p_r + \sigma) u_\mu u_\nu - \sigma k_\mu k_\nu. \quad (2.2)$$

The variables p_r , ρ , and σ depict, respectively, the radial pressure, the energy density, and the anisotropic factor. $g_{\mu\nu}$, u_μ , and k_μ represent the spacetime metric tensor, the fluid's 4-velocity, unit radial vector, respectively. In addition, the 4-velocity and the unit radial vector follow the equalities:

$$u_\mu u^\mu = -1, \quad k_\mu k^\mu = 1, \quad \text{and} \quad k_\mu u^\mu = 0. \quad (2.3)$$

To analyze the static equilibrium configuration of spherically symmetric static compact stars, we consider the line element in the Schwarzschild-like coordinates (t, r, θ, ϕ) as follows:

$$ds^2 = -e^{2\Psi} dt^2 + e^{2\Lambda} dr^2 + r^2 (d\theta^2 + \sin^2 \theta d\phi^2), \quad (2.4)$$

where $\Psi = \Psi(r)$ and $\Lambda = \Lambda(r)$ are functions of the radial coordinate r only.

Replacing the energy-momentum tensor (2.2) and the metric (2.4) on the Einstein field equation, we derive the hydrostatic stellar structure equations:

$$\frac{dp_r}{dr} = -\frac{\rho m}{r^2} \left[1 + \frac{p_r}{\rho} \right] \left[1 + \frac{4\pi r^3 p_r}{m} \right] e^{2\Lambda} + \frac{2\sigma}{r}, \quad (2.5)$$

$$\frac{dm}{dr} = 4\pi r^2 \rho, \quad (2.6)$$

$$\frac{d\Psi}{dr} = -\frac{1}{p_r + \rho} \frac{dp_r}{dr} + \frac{2\sigma}{r(p_r + \rho)}, \quad (2.7)$$

with

$$e^{2\Lambda} = \left(1 - \frac{2m}{r} \right)^{-1}. \quad (2.8)$$

As usual, the parameter m represents the mass within the sphere radius r . Eq. (2.5) is known as the hydrostatic equilibrium equation, it is also known as the Tolman-Oppenheimer-Volkoff equation [38, 39], modified from its standard form to include the anisotropic factor σ , see Ref. [40].

Eqs. (2.5)-(2.7) are integrated from the center ($r = 0$) to the surface of the star ($r = R$). This solution starts at the center of the star $r = 0$, where:

$$m(0) = 0, \quad \rho(0) = \rho_c, \quad p_r(0) = p_{rc}, \quad \sigma(0) = 0, \quad \text{and} \quad \Psi(0) = \Psi_c, \quad (2.9)$$

and the star's surface is determined by $p_r(r = R) = 0$. Moreover, the interior line element connects smoothly with the exterior Schwarzschild vacuum metric at the star's surface. Thus, the inner and outer potential metric functions are connected by the relation:

$$e^{2\Psi(R)} = e^{-2\Lambda(R)} = 1 - \frac{2M}{R}, \quad (2.10)$$

with M representing the total mass of the star. Eq. (2.10) depicts the boundary condition of $\Psi(R)$ at the star's surface.

2.2 Nonradial perturbation equations

The study of the nonradial oscillations is investigated by decomposing the perturbed metric into a background metric $g_{\mu\nu}^{(0)}$, whose components are found in Eq. (2.4), plus the metric perturbation $h_{\mu\nu}$. This decomposition can be placed into the form:

$$g_{\mu\nu} = g_{\mu\nu}^{(0)} + h_{\mu\nu}. \quad (2.11)$$

In pulsating compact stellar configurations, the fluid spacetime dynamics are described by the perturbed Einstein field equation and conservation of the energy-momentum tensor

$$\delta G_{\varphi}^{\mu} = 8\pi\delta T_{\varphi}^{\mu}, \quad (2.12)$$

$$\delta(\nabla_{\mu}T_{\varphi}^{\mu}) = 0, \quad (2.13)$$

with

$$\delta G_{\varphi}^{\mu} = g^{(0)\mu\beta}\delta R_{\varphi\beta} - \frac{1}{2}\delta_{\varphi}^{\mu}\left(g^{(0)\alpha\beta}\delta R_{\alpha\beta} - h^{\alpha\beta}R_{\alpha\beta}^{(0)}\right) - \frac{1}{2}g^{(0)\mu\beta}h_{\varphi\beta}R^{(0)} - h^{\mu\beta}G_{\varphi\beta}^{(0)}, \quad (2.14)$$

$$\begin{aligned} \delta T_{\varphi}^{\mu} &= (\delta\rho + \delta p_r + \delta\sigma)u^{\mu}u_{\varphi} + (\rho + p_r + \sigma)\delta u^{\mu}u_{\varphi} + (\rho + p_r + \sigma)u^{\mu}\delta u_{\varphi} + \delta p_r g_{\nu\varphi}^{(0)}g^{(0)\mu\nu} \\ &+ \delta\sigma g_{\nu\varphi}^{(0)}g^{(0)\mu\nu} + (p_r + \sigma)h_{\nu\varphi}g^{(0)\mu\nu} - (p_r + \sigma)g_{\nu\varphi}^{(0)}h^{\mu\nu} - \delta\sigma g_{\nu\varphi}^{(0)}k^{\mu}k^{\nu} - \sigma h_{\varphi\nu}k^{\mu}k^{\nu} - \sigma g_{\varphi\nu}^{(0)}\delta k^{\mu}k^{\nu} \\ &- \sigma g_{\varphi\nu}^{(0)}k^{\mu}\delta k^{\nu}. \end{aligned} \quad (2.15)$$

To investigate the effects of anisotropy on the fluid pulsation mode emitted by compact stars, following [41] and adopting the Regge and Wheeler [42] gauge, the metric perturbation $h_{\mu\nu}$ for a given even-parity spherical harmonic function $Y_{\ell m}(\theta, \phi)$ is given by

$$h_{\mu\nu} = \begin{pmatrix} He^{2\Psi} & H_1 & 0 & 0 \\ H_1 & He^{2\Lambda} & 0 & 0 \\ 0 & 0 & Kr^2 & 0 \\ 0 & 0 & 0 & Kr^2 \sin^2\theta \end{pmatrix} Y_{\ell m}, \quad (2.16)$$

with H , H_1 , and K depending on t and r . Through the non-zero components of the perturbed Einstein field equation (2.12) and the perturbed components of the conservation of the energy-momentum tensor ($\delta(\nabla_{\nu}T_1^{\nu}) = 0$ and $\delta(\nabla_{\nu}T_2^{\nu}) = 0$), the nonradial oscillation equations for a general anisotropic profile can be obtained; see Eqs. (A.15)-(A.21). Since we concentrate our attention on normal modes, following Ref. [43, 44], we employ $H = r^{\ell}\tilde{H}e^{i\omega t}$, $H_1 = i\omega r^{\ell+1}\tilde{H}_1e^{i\omega t}$, $K = r^{\ell}\tilde{K}e^{i\omega t}$, $W = r^{\ell+1}\tilde{W}e^{i\omega t}$, and $V = r^{\ell}\tilde{V}e^{i\omega t}$; where the functions \tilde{H} , \tilde{H}_1 , \tilde{K} , \tilde{W} , and \tilde{V} depend on r and ω represents the oscillation eigenfrequency. By using these five equalities and introducing the function \tilde{X} defined by

$$\tilde{X} = \left(1 + \frac{\partial\sigma}{\partial p_r}\right)^{-1} \left[\omega^2(\rho + p_r + \sigma)\tilde{V}e^{-\Psi} - (\rho + p_r)\frac{\tilde{H}}{2}e^{\Psi} + e^{\Psi+2\Lambda}\tilde{H}\frac{\partial\sigma}{\partial g_{11}} \right] - \frac{p'_r\tilde{W}}{re^{\Lambda-\Psi}}, \quad (2.17)$$

equations (A.15)-(A.21) yield

$$\tilde{H}'_1 = \frac{e^{2\Lambda}}{r} \left[\tilde{H} + \tilde{K} + 16\pi(\rho + p_r + \sigma)\tilde{V} \right] - \frac{\tilde{H}_1}{r} \left[\ell + 1 + \frac{2me^{2\Lambda}}{r} + 4\pi r^2(p_r - \rho)e^{2\Lambda} \right], \quad (2.18)$$

$$\tilde{K}' = \frac{\tilde{H}}{r} + \frac{\ell(\ell+1)}{2r} \tilde{H}_1 - \frac{\tilde{K}}{r} (\ell + 1 - \Psi' r) + 8\pi(\rho + p_r) \frac{e^\Lambda \tilde{W}}{r}, \quad (2.19)$$

$$\begin{aligned} \tilde{W}' = & -(\ell+1) \frac{\tilde{W}}{r} + r e^\Lambda \left[\frac{e^{-\Psi} \tilde{X}}{p_r + \rho} \frac{d\rho}{dp_r} - \ell(\ell+1) \frac{(p_r + \rho + \sigma)}{(p_r + \rho)} \frac{\tilde{V}}{r^2} - \frac{\tilde{H}}{2} \right. \\ & \left. - \frac{2\sigma \tilde{W}}{e^\Lambda r^2 (p_r + \rho)} - \frac{(p_r + \rho + \sigma) \tilde{K}}{(p_r + \rho)} \right], \end{aligned} \quad (2.20)$$

$$\begin{aligned} \tilde{X}' = & \tilde{W} \frac{e^\Psi}{r} \left[(p_r + \rho) \left[-4\pi(\rho + p_r) e^\Lambda - \omega^2 e^{\Lambda-2\Psi} + \left[\frac{e^{-\Lambda} \Psi'}{r^2} \right]' r^2 \right] + \frac{2}{r} \left[\frac{3\sigma}{r} + p'_r \frac{\partial \sigma}{\partial p_r} - \sigma' \right. \right. \\ & \left. \left. - 2\sigma \Psi' + \frac{2\sigma^2}{r(p_r + \rho)} \right] e^{-\Lambda} \right] - \tilde{H}_1 \frac{e^\Psi}{2} \left[(p_r + \rho) \left[\frac{\ell(\ell+1)}{2r} + e^{-2\Psi} r \omega^2 \right] + \frac{\ell(\ell+1)\sigma}{r} \right] \\ & + \tilde{H} \left[\frac{e^\Psi}{2} (p_r + \rho) \left[\Psi' - \frac{1}{r} \right] - \frac{2}{r} e^{\Psi+2\Lambda} \frac{\partial \sigma}{\partial g_{11}} \right] + \tilde{K} \left[(p_r + \rho) \frac{e^\Psi}{2} \left[\frac{1}{r} - 3\Psi' \right] + \sigma e^\Psi \left[\frac{3}{r} \right. \right. \\ & \left. \left. - 2\Psi' + \frac{2\sigma}{r(p_r + \rho)} \right] \right] - \tilde{X} \left[\frac{\ell}{r} + \frac{d\rho}{dp_r} \frac{2\sigma}{r(p_r + \rho)} - \frac{2}{r} \frac{\partial \sigma}{\partial p_r} \right] + \tilde{V} \frac{e^\Psi}{r^2} \ell(\ell+1) [-(p_r + \rho)\Psi' \\ & + \frac{2\sigma}{r}] \left[1 + \frac{\sigma}{p_r + \rho} \right], \end{aligned} \quad (2.21)$$

$$\begin{aligned} \tilde{H} \left[3m + \frac{1}{2}(\ell+2)(\ell-1)r + 4\pi p_r r^3 \right] = & \tilde{H}_1 \left[\omega^2 r^3 e^{-2(\Psi+\Lambda)} - \frac{\ell(\ell+1)}{2} (m + 4\pi r^3 p_r) \right] \\ & + \tilde{K} \left[\frac{1}{2}(\ell+2)(\ell-1)r - \omega^2 r^3 e^{-2\Psi} - \frac{e^{2\Lambda}}{r} (m + 4\pi r^3 p_r) (3m - r + 4\pi r^3 p_r) \right] - 8\pi e^{-\Psi} \tilde{X} r^3 \\ & - 16\pi e^{-\Lambda} \sigma \tilde{W} r. \end{aligned} \quad (2.22)$$

Here, the anisotropic profile employed depends on the fluid and spacetime variables of the form $\sigma = \sigma(p_r, g_{11})$ with $p_r = p_r(\rho)$; see, e.g., [45, 46]. Eqs. (2.17)-(2.22) can be reduced to the fourth-order system of linear equations presented in [44] by taking $\tilde{H} \rightarrow -H$, $\tilde{H}_1 \rightarrow -H_1$, $\tilde{K} \rightarrow -K$, and $\sigma = 0$; review also [47]. In addition, Eqs. (2.20) and (2.21) differ from the respective equations derived in Ref. [36] in all terms where the anisotropic factor appears; however, these equations are in concordance with those reported in Ref. [33-35].

To solve Eqs. (2.17)-(2.22), some conditions at the center ($r = 0$) and at the surface of the star ($r = R$) are required. In the center of the star, as is realized in the isotropic case [43, 44], regularity conditions of the perturbative variables are imposed. These conditions are found by expanding the fluid variables and the spacetime perturbations by Taylor power series near $r = 0$. These expansions, together with the perturbation equations (2.17)-(2.22) reduced through these expansions, are shown in Appendix B. In turn, outside the stellar structure configuration $r \geq R$, the fluid variables p_r , ρ , and σ and the fluid perturbation quantities W and V are zero and $m = M$. In addition, such as is realized in [19], we replace the variables

\tilde{H}_1 and \tilde{K} with the new ones Z and dZ/dr^* through the equalities:

$$\tilde{K} = \frac{n(n+1)r^2 + 3nMr + 6M^2}{r^{\ell+2}(nr + 3M)}Z + \frac{1}{r^{\ell+2}}\frac{dZ}{dr^*}, \quad (2.23)$$

$$\tilde{H}_1 = \frac{nr^2 - 3nMr - 3M^2}{r^{\ell+1}(r - 2M)(nr + 3M)}Z + \frac{r^{1-\ell}}{(r - 2M)}\frac{dZ}{dr^*}, \quad (2.24)$$

giving rise to the Zerilli equation [48–50]. In Eqs. (2.23) and (2.24), $n = (\ell - 1)(\ell + 2)/2$ and r^* is the so-called ‘‘tortoise’’ coordinate, which is related to the radial coordinate r through the relation:

$$r^* = r + 2M \ln \left(\frac{r}{2M} - 1 \right). \quad (2.25)$$

At the star’s surface ($r = R$), the Lagrangian perturbation Δp_r must vanish, i.e.,

$$\Delta p_r = -r^\ell e^{-\Psi} \tilde{X} = 0, \quad (2.26)$$

thus implying $\tilde{X}(r = R) = 0$. Each mode solution is uniquely associated with a specific (ℓ, ω) pair; however, not every combination of (ℓ, ω) corresponds to a valid mode solution, since the spectrum is discrete.

2.3 Tidal deformability

The investigation of tidal Love numbers has emerged as a key aspect in understanding binary systems consisting of compact stars. In these systems, the gravitational pull exerted by one star induces tidal distortions in its companion. Such deformations, arising from external tidal forces, are characterized by the dimensionless tidal deformability parameter Λ , which is defined as

$$\Lambda = \frac{2k_2}{3C^5}. \quad (2.27)$$

In this equation, $C = M/R$ represents the stellar compactness, and k_2 is the quadrupolar Love number, which can be written as

$$k_2 = \frac{8C^5}{5}(1 - 2C)^2[2 + C(y_R - 1) - y_R] \times \{2C[6 - 3y_R + 3C(5y_R - 8)] + 4C^3[13 - 11y_R + C(3y_R - 2) + 2C^2(1 + y_R)] + 3(1 - 2C^2) \times [2 - y_R + 2(y_R - 1)] \ln(1 - 2C)\}^{-1}, \quad (2.28)$$

where $y_R = y(r = R)$. The function $y(r)$ follows the Riccati-type differential equation

$$y'r + y^2 + y(K_0 r - 1) + K_1 r^2 = 0, \quad (2.29)$$

with coefficients

$$K_0 = \frac{2m}{r^2}e^{2\Lambda} + 4\pi e^{2\Lambda}(p_r - \rho)r + \frac{2}{r}, \quad (2.30)$$

$$K_1 = 4\pi e^{2\Lambda} \left[4\rho + 8p_r + 4\sigma + \frac{p_r + \rho}{Ac_s^2}(c_s^2 + 1) \right] - \frac{6}{r^2}e^{2\Lambda} - 4\Psi'^2, \quad (2.31)$$

where $c_s^2 = \frac{dp_r}{d\rho}$ and $A = \frac{dp_t}{dp_r}$. Additional information can be found in Ref. [46] and the references therein.

3 Equation of state and anisotropic profile

3.1 Equation of state

In the outer layers of a compact object, the composition of matter evolves from nuclei embedded in an electron sea in the outer crust to progressively more neutron-rich matter in its most inner regions. In this low density regions, the EOS has been derived from many-body calculations using phenomenological potentials, typically including both two and three nucleon interactions [51]. Recently, chiral effective field theory (CEFT) has provided a systematic framework for expanding nuclear forces at low momenta, naturally explaining the hierarchy among two-body, three-body, and weaker higher-body interactions [52–57]. At present, microscopic calculations based on CEFT interactions allow a reliable determination of the properties of neutron star matter up to the nuclear saturation density n_0 .

In the inner regions of a neutron star, at moderate high densities, the EOS of cold quark matter can be obtained in the framework of perturbative QCD. The resulting EOS depends on an unphysical parameter, namely the renormalization scale associated with the chosen scheme. Although this dependence decreases order by order in perturbation theory, it provides a practical estimate of the contributions from yet uncalculated higher-order terms and thus serves as a quantitative measure of the intrinsic theoretical uncertainty [58]. Here we use the numerical EOS derived in [59] which is well represented by a fitting function for the pressure in terms of the baryon chemical potential μ_B [60]. Fixing the strong coupling constant and the strange quark mass at arbitrary reference scales (using lattice and experimental data), the EOS of quark matter in β -equilibrium reads

$$P_{QCD}(\mu_B) = P_{SB} \left[c_1 - \frac{a(X)}{(\mu_B/GeV) - b(X)} \right], \quad (3.1)$$

with $P_{SB} = \frac{3}{4\pi^2}(\mu_B/3)^4$, $a(X) = d_1 X^{-\nu_1}$ and $b(X) = d_2 X^{-\nu_2}$, where X is a parameter proportional to the renormalization scale of the theory (typically varied from 1 to 4). The parameters are $c_1 = 0.9008$, $d_1 = 0.5034$, $d_2 = 1.452$, $\nu_1 = 0.3553$ and $\nu_2 = 0.9101$. These formulae reproduce the full three-loop pressure correctly, the quark number density and the speed of sound to per cent accuracy for baryon chemical potentials up to 6 [GeV] [58, 60].

To construct the EOS over the entire density range, we proceed as follows. For densities below $1.1n_0$, the CEFT EOS of [61] is used. At baryon chemical potentials above 2.6 [GeV], where the relative uncertainty of the quark matter EOS is as large as the nuclear matter one at $n = 1.1n_0$, the expression of Eq. (3.1) is used. Between these two regions, it is assumed that the EOS is well approximated by an interpolating polytrope built from two monotropes of the form

$$P_i(\mu_B) = k_i \left(n_i^{\gamma_i - 1} + \frac{\gamma_i - 1}{k_i \gamma_i} (\mu_B - \mu_{B,i}) \right)^{\frac{\gamma_i}{\gamma_i - 1}}, \quad (3.2)$$

where $i = 1, 2$, with $\mu_{B,i}$ and n_i being the baryon chemical potential and the baryon density respectively. These functions are connected smoothly and also allowing a density jump at the matching point of the two monotropes due to a first-order phase transition. In this work we will use the representative EOS III given in [58], which satisfies the requirement that the EOS is able to support a two solar mass star (to be in agreement with recent mass determinations using pulsar timing [62, 63]).

n/n_0	p	ρ	μ	c_s^2
1.1	3.542	168.5	0.9775	0.15
1.3	12.13	200.4	1.022	0.42
1.5	34.81	234.5	1.122	0.95
1.7	42.24	270.9	1.151	0.19
1.9	49.44	308.1	1.176	0.20
2.1	56.96	346.2	1.200	0.20
2.3	64.79	384.9	1.222	0.20
2.5	72.90	424.4	1.243	0.21
2.7	81.29	464.5	1.263	0.21
2.9	89.94	505.2	1.283	0.21
3.1	98.84	546.5	1.301	0.22
3.3	108.0	588.5	1.319	0.22
3.5	117.4	631.0	1.336	0.22
3.7	127.0	674.0	1.353	0.22
3.9	136.8	717.5	1.369	0.23

Table 1. The representative equation of state III. The baryon number density n is given in units of the saturation density $n_0 = 0.16$ [fm³], while the pressure p and the energy density ρ are given in [MeV/fm³]. The solid horizontal line indicates the transition between the two monotropes [58].

3.2 Anisotropic profile

To describe the anisotropic profile, we employ the quasilocal anisotropic profile. As described in [64], it depends on the fluid and spacetime variables of the form $\sigma = \sigma(p_r, g_{11})$. Thus, this equation is given by:

$$\sigma = \alpha p_r \left(1 - \frac{1}{g_{11}} \right)^n, \quad (3.3)$$

where α is a dimensionless anisotropic constant and $g_{11} = e^{2\Lambda}$. The anisotropy model (3.3) was used, e.g., with $n = 1$, to analyze the effects of the anisotropy on the radial pulsation modes of polytropic stars [64, 65] and strange quark stars [66], nonradial oscillation modes within Cowling approximation of neutron stars [45] and strange quark stars [46], magnetic field structure [67], and slowly rotating neutron stars [68, 69] and, with $n = 2$, to investigate its influence on quasinormal modes [33, 34] and on the fundamental oscillation modes of neutron stars [35]. In the present work, we consider values of α within the interval between -1 and 1 .

For the anisotropic profile (3.3), we note that

$$\frac{\partial \sigma}{\partial g_{11}} = \frac{2\alpha p_r}{g_{11}^2} \left(1 - \frac{1}{g_{11}} \right), \quad \frac{\partial \sigma}{\partial p_r} = \alpha \left(1 - \frac{1}{g_{11}} \right)^2, \quad \text{and} \quad \frac{\partial \sigma}{\partial \rho} = \frac{\partial p_r}{\partial \rho} \frac{\partial \sigma}{\partial p_r}. \quad (3.4)$$

It is important to highlight these factors since they appear in Eqs. (2.17)–(2.22). In this way, the set of equations to analyze nonradial oscillations is complete.

4 Anisotropic effects on the equilibrium, frequency of oscillations, and tidal deformability

4.1 General remarks

For nonradial oscillations mode: To determine the fundamental mode frequency, we choose a suitable trial Newtonian value $\omega_{Newt} = \sqrt{(M/R^3)2l(l-1)/(2l+1)}$ as a starting point, as made in Ref. [43]. Then we start the integration process within the stellar interior. First, we construct three linearly independent solutions that satisfy the regularity conditions at the star's center and numerically integrate them outward from $r = 0$ to the midpoint at $R/2$. Next, we construct two additional linearly independent solutions that meet the boundary conditions at the stellar surface, and integrate them inward from $r = R$ to $R/2$. Finally at $R/2$, we combine these five solutions, in a way that ensures the resulting function satisfies the boundary conditions at both the center and the surface, completing the computation of the mode within the star.

The next step is to solve the Zerilli equation in the exterior region of the star. To accomplish this, we first determine the boundary values at the stellar surface for both the Zerilli function and its radial derivative. These can be extracted from the values of the metric perturbation functions $H(R)$ and $K(R)$ obtained through the interior integration. With these boundary conditions at $r = R$, the Zerilli equation is integrated outward in terms of the tortoise coordinate r^* . In the asymptotic regime, where $r^* \rightarrow \infty$, the general solution of the Zerilli equation can be represented as a linear combination of ingoing and outgoing waves, as can be found in Ref. [70].

To determine the quasi-normal mode frequencies, we have to integrate the Zerilli equation from the surface of the star to a sufficiently large radial coordinate, typically taken as $r_\infty \approx 50\omega^{-1}$ (During that integration, ω is treated as a real parameter in both the interior and exterior regions). The physical boundary condition at infinity imposes that only outgoing gravitational waves should be present. Therefore, the problem of finding quasi-normal mode frequencies reduces to locating the complex roots as done in [71].

This procedure is repeated iteratively: the real part of the estimated root is used as the new trial input in the next integration cycle. The iterations continue until the real part of the frequency converges to within one part in 10^8 between successive steps. Additionally, once convergence is reached, the imaginary part of the frequency $\text{Im}(\omega)$ yields the damping timescale of the mode.

For tidal deformability: To examine how anisotropy influences the tidal deformability of neutron stars, we numerically integrate the stellar structure equations (2.5)-(2.7) together with the tidal deformability equation (2.29) from the center of the star ($r = 0$) to its surface ($r = R$). Specifically, Eqs. (2.5)-(2.7) are first solved using the fourth-order Runge-Kutta method for various choices of the anisotropy parameter α and central energy density ρ_c . This step provides the radial profiles for p_r , σ , ρ , m , and Ψ . Next, Eq. (2.7) is handled via the shooting method: an initial trial for Ψ_c at the center is supplied, and if the resulting solution does not satisfy the boundary condition given in equation (2.7), Ψ_c is iteratively adjusted until convergence is achieved. With the consistent Ψ_c determined, the tidal deformability equation (2.29) is then integrated outward from $r = 0$ to $r = R$, ensuring a self-consistent solution for each selected pair of α and ρ_c . Once the deformability function $y(r)$ is known, the value of $y(r = R)$ is determined by means of Eq. (2.28), which finally allows us to calculate the dimensionless deformability parameter (2.27).

4.2 Equilibrium configurations and frequency of oscillations

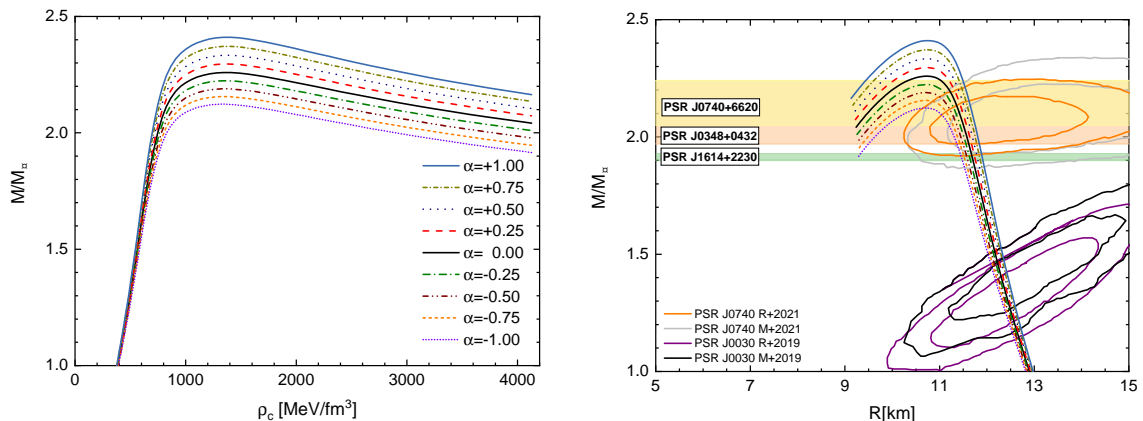


Figure 1. The total gravitational mass, in Sun’s masses, against the central energy density and as a function of the total radius are plotted on the left and right panels, respectively. In both panels, nine different anisotropic parameters α are employed. The solid purple and black curves indicate the 95% confidence intervals for the masses and radii of PSR J0030 + 0451 [72, 73], while the orange and gray curves show the same for PSR J0740 + 6620 [74, 75], both measured by the NICER collaboration. In all cases, the outer lines offer a greater likelihood of containing the true value but with lower precision, whereas the inner lines provide higher accuracy but with lower statistical coverage.

The normalized mass with Solar mass as a function of the central energy density and versus the radius is presented on the left and right panels of Fig. 1, respectively, for nine different anisotropic parameters. We consider central energy densities in the range 400–4200, [MeV/fm³]. As shown in the left panel, the stellar mass increases monotonically with increasing central energy density up to a maximum mass configuration. Beyond this point, the mass decreases with further increases in ρ_c . In the right panel, all mass–radius curves show that the mass increases as the radius decreases, up to the maximum-mass configuration. At this point, the curves bend counterclockwise, and the mass subsequently decreases with further changes in the radius. At this panel, the masses–radii relation reported by NICER from compact stars PSR J0030 + 0451 [72, 73] and PSR J0740 + 6620 [74, 75] are also presented. The corresponding bands of the pulsars PSR J0740 + 6620 [76], PSR J0348 + 0432 [63], and PSR J1614 + 2230 [62], respectively marked by light yellow, light orange, and light green colors, are also shown in the mass–radius diagram.

The effect of anisotropic pressure on mass and radius can also be observed in Fig. 1. Upon examining the maximum mass and its corresponding total radius, it becomes evident that the mass varies significantly with changes in α ; however, the total radius exhibits only a small variation. Once α exceeds (falls) zero, the growth (diminution) of α requires the star to attain a higher (lower) maximum mass to achieve equilibrium. Moreover, the increase (decrease) in mass with σ can be understood by noting the change of σ with the parameter α . Greater (Lesser) anisotropy σ supports higher (lower) fluid pressure, enabling stars with larger (smaller) masses to resist collapse.

In addition, based on the curves that pass through the confidence regions reported by NICER in the mass–radius plane, it can be inferred that the model under consideration is consistent with current observational constraints. The overlap between the equilibrium configurations and the ellipses corresponding to the observed pulsars indicates that the stellar

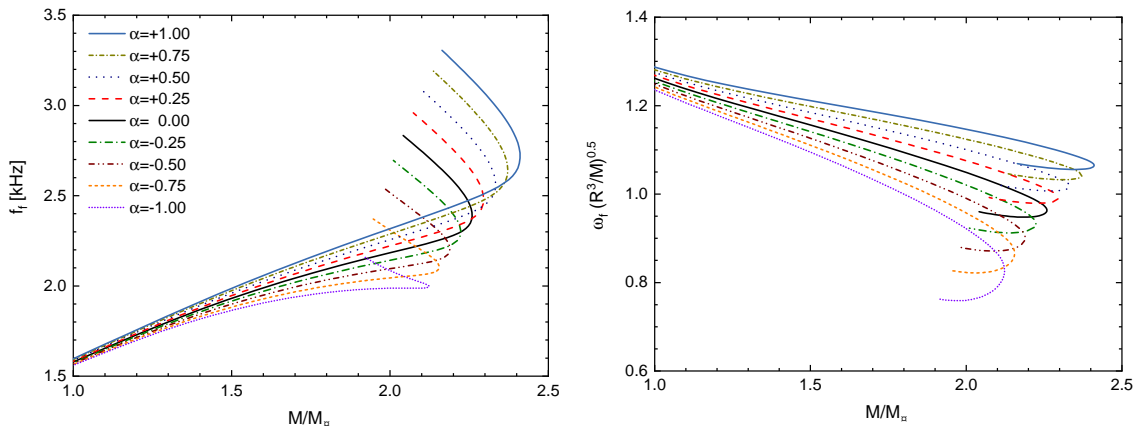


Figure 2. The f -mode frequency of oscillations and the normalized ω_f with the average density $(M/R^3)^{0.5}$ against the total mass are presented on the left and right panels, respectively. In both panels, nine different anisotropic parameters α are used.

configurations predicted by the present model simultaneously reproduce the inferred masses and radii within the statistical uncertainties. This comparison allows us to constrain the permissible range of the model’s physical parameters, thereby providing additional restrictions on the degree of anisotropy and, more generally, on the equation of state of the stellar fluid.

The f -mode nonradial oscillation frequency and the eigenfrequency normalized by the square root of the average density, $(\sqrt{M/R^3})$, as functions of the total mass, are shown in the left and right panels of Fig. 2, respectively, for selected values of the anisotropy parameter α .

In the left panel, all curves show that the f -mode frequency increases monotonically with the total mass up to the maximum-mass configuration. After this point, the curve turns counterclockwise, so that the fundamental frequency of the oscillation begins to increase with the decrease in total mass. The influence of anisotropy on the fluid pulsation mode is also evident. From the f -mode frequency versus M/M_\odot curves, in certain mass ranges, the f -mode frequency increases or decreases in correspondence with an increase or decrease in α .

In the right panel, in all the curves presented, up to the point of maximum mass, the relationship between $\omega_f \sqrt{R^3/M}$ and M/M_\odot produces an almost linear behavior. Beyond the maximum mass value, the curve bends clockwise and $\omega_f \sqrt{R^3/M}$ starts to increase with M/M_\odot . As noted in [66], variations in the oscillation frequency are linked to changes in the radial fluid pressure induced by anisotropy.

Table 2 presents the mass, radius, compactness, f -mode pulsation frequency, and the oscillation eigenfrequency normalized with the mean density, for compact objects for the central energy densities 400 [MeV/fm³] and 600 [MeV/fm³] and five values of anisotropic parameters α . It can be noted that, when varying α from -1.0 to $+1.0$, the mass, radius, compactness, f -mode, and the normalized oscillation eigenfrequency change respectively in almost +4.41%, +9.60%, +0.42%, +7.32%, and +4.44% for $\rho_c = 400$ [MeV/fm³] and in +14%, +18%, +1.4%, +23%, and +11% for $\rho_c = 600$ [MeV/fm³]. Thus, for a central energy density interval, we note that when α increases, the mass, radius, compactness, the f -mode frequency, and the normalized eigenfrequency ω_f rise. From these results, along with those shown in Figures 1 and 2, we see that as the star’s mass and radius increase, the oscillation mode f also increases.

ρ_c [MeV/fm ³]	α	M/M_\odot	R [km]	M/R	f_f [kHz]	$\omega_f \sqrt{R^3/M}$
400	-1.0	1.0171	12.792	0.1174	1.5726	1.2305
	-0.5	1.0277	12.815	0.1184	1.5902	1.2413
	0.0	1.0386	12.838	0.1194	1.6082	1.2523
	+0.5	1.0499	12.863	0.1205	1.6268	1.2634
	+1.0	1.0612	12.888	0.1216	1.6458	1.2749
600	-1.0	1.5498	11.954	0.1914	1.8863	1.0802
	-0.5	1.5819	11.995	0.1947	1.9414	1.1061
	0.0	1.6159	12.038	0.1982	1.9989	1.1328
	+0.5	1.6519	12.083	0.2019	2.0586	1.1602
	+1.0	1.6902	12.130	0.2057	2.1187	1.1876

Table 2. The mass M/M_\odot , radius R , compactness M/R , f -mode oscillation frequency, and eigenfrequency normalized with the mean density $\omega_f \sqrt{R^3/M}$ for neutron stars with two different central energy densities and different values of α .

4.3 On the detectability of the fundamental mode signal

A core-collapse supernova (CCSN) is a violent explosion marking the end of the life of a massive star with $M \gtrsim 8M_\odot$. Once the stellar core exceeds the effective Chandrasekhar limit ($\sim 1.4M_\odot$), it becomes gravitationally unstable and collapses to nuclear densities. The ensuing collapse drives a shock wave that triggers the CCSN explosion. Gravitational waves and neutrinos are emitted directly from the collapsing core, providing unique probes of the physical mechanisms underlying CCSN dynamics. Following the explosion, a hot proto-neutron star may form; during its early evolution, the gravitational-wave spectrum is dominated by the fundamental f -mode and the first pressure mode p_1 [77]. A typical CCSN releases a total energy of $\sim 10^{53}$ erg ($\sim 0.056M_\odot$), and part of this energy may be radiated through f -mode oscillations [77, 78].

Let us consider the detection of gravitational waves associated with the fundamental oscillation mode of a magnetar formed after a supernova explosion. It is well established that when a gravitational wave reaches the detector, the signal takes the following form:

$$h(t) = h e^{-t/\tau} \sin[2\pi f t], \quad (4.1)$$

with f being the fundamental mode frequency, τ is the damping time and the gravitational wave amplitude h is given by

$$h \sim A \left(\frac{E_{gw}}{10^{-6} M_\odot} \right)^{1/2} \left(\frac{10 \text{ kpc}}{d} \right) \left(\frac{1 \text{ kHz}}{f} \right) \left(\frac{1 \text{ ms}}{\tau} \right)^{1/2}, \quad (4.2)$$

where $A = 2.4 \times 10^{-20}$, E_{gw} is the energy released through the fundamental mode and d is the distance to the source [78, 79].

The signal-to-noise ratio at the detector reads [78, 79]

$$\left(\frac{S}{N} \right)^2 = \frac{4Q_F^2}{1 + 4Q_F^2} \frac{h^2 \tau}{2S_n}. \quad (4.3)$$

Here, $Q_F \equiv \pi f \tau$ is the quality factor and S_n is the noise power spectral density.

ρ_c [MeV/fm ³]	α	τ [ms]	E_{gw}^{LV} [$10^{-7}M_\odot$]	E_{gw}^{ET} [$10^{-10}M_\odot$]
400	-1.0	445.450	0.8582	2.1454
	-0.5	419.308	0.8775	2.2194
	0.0	394.512	0.8974	2.2435
	+0.5	371.023	0.9183	2.2958
	+1.0	348.620	0.9399	2.3498
600	-1.0	225.026	1.2347	3.0868
	-0.5	192.603	1.3079	3.2698
	0.0	164.723	1.3865	3.4663
	+0.5	140.722	1.4705	3.3676
	+1.0	120.055	1.5576	3.8941

Table 3. The damping time τ for neutron stars, the energy required to excite the fundamental mode, E_{gw}^{LV} and E_{gw}^{ET} , for the signal to be detectable by Advanced LIGO-Virgo and the Einstein Telescope, respectively. For this result, we considered the source at $d \sim 10$ [kpc], a signal-to-noise ratio $S/N \sim 5$, two different central densities, and different values of α .

From Eqs. (4.2) and (4.3), the energy radiated by the fundamental mode is given by

$$\left(\frac{E_{gw}}{M_\odot}\right) = BC \left(\frac{S}{N}\right)^2 \left(\frac{d}{10\text{kpc}}\right)^2 \left(\frac{f}{1\text{kHz}}\right)^2 \left(\frac{S_n}{1\text{Hz}^{-1}}\right), \quad (4.4)$$

where $B = 3.47 \times 10^{36}$ and $C = (1 + 4Q_F^2)/4Q_F^2$. In the following, we estimate the minimum energy that must be emitted in order to achieve a signal-to-noise ratio (S/N) greater than 5, for a source that could be observed within our galaxy, i.e, at $d \sim 10$ [kpc]

In Table 3, we show the minimum energy required for the fundamental mode to be detected. For this objective, we consider two detectors; the first one is Advanced LIGO-Virgo with a sensitivity of $S_n^{1/2} \sim 2 \times 10^{-23} [\text{Hz}]^{-1/2}$ at \sim [kHz] [1], and the second one is the Einstein telescope with a sensitivity $S_n^{1/2} \sim 10^{-24} [\text{Hz}]^{-1/2}$ at a similar frequency band [80].

For a fixed central energy density $\rho_c = 600$ [MeV/fm³], varying the anisotropy from $\alpha = -1.0$ to $\alpha = +1.0$ produces measurable shifts in the f -mode properties and the GW energy needed for detectability. For $\alpha = -1.0$ we obtain $M = 1.5498 M_\odot$, $f = 1.8863$ [kHz], $\tau = 225.026$ [ms], with detection thresholds $E_{gw}^{LV} > 1.2347 \times 10^{-7} M_\odot$ (Advanced LIGO/Virgo, $S/N > 5$) and $E_{gw}^{ET} > 3.0868 \times 10^{-10} M_\odot$ (Einstein Telescope, $S/N > 5$). For $\alpha = +1.0$ we find $M = 1.6902 M_\odot$, $f = 2.1187$ [kHz], $\tau = 120.055$ [ms], and thresholds $E_{gw}^{LV} > 1.5576 \times 10^{-7} M_\odot$ and $E_{gw}^{ET} > 3.8941 \times 10^{-10} M_\odot$. This systematic response of (f, τ, E_{gw}) to α -combined with independent constraints on M and R -provides a practical diagnostic for future GW asteroseismology: precise measurements can bound the level of anisotropy and, given the higher compactness and typically higher f -mode frequencies expected for neutron stars, help discriminate neutron from strange-matter compositions.

4.4 Tidal deformability

Fig. 3 plots, in its left and right panels respectively, the dimensionless tidal deformability Λ against the total mass M/M_\odot and the oscillation frequencies of the fundamental mode f_f as a function of the dimensionless tidal deformability Λ for several choices of the anisotropy parameter α . These curves are compared with the observational range for $\Lambda_{1.4} = 190_{-120}^{+390}$ reported by LIGO-Virgo [81]. In the left panel, the tidal deformability decreases monotonically as the total mass increases, up to the maximum-mass configuration. After this point,

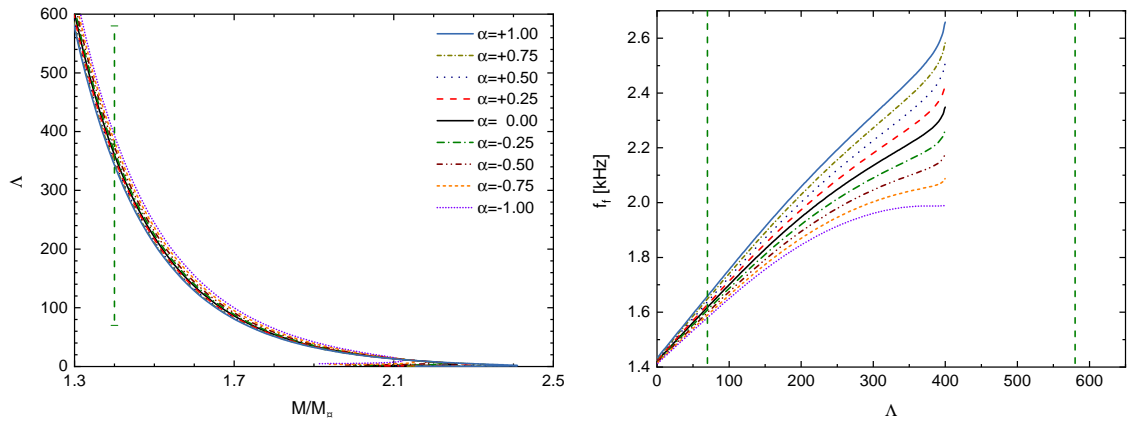


Figure 3. Left: Dimensionless tidal deformability against the total mass for different values of α . Right: Oscillation frequency f_f as a function of the dimensionless tidal deformability for nine values of α . In both panels, the vertical dashed line depicts dimensionless tidal deformability $\Lambda_{1,4} = 190^{+390}_{-120}$ from the event GW170817 reported by LVC in Ref. [81].

the curves bend clockwise, and the tidal deformability continues to decrease as the total mass diminishes. Additionally, the influence of anisotropy on the deformability response is clearly seen: when α is positive, the calculated Λ values are lower for a given mass, whereas negative α leads to larger values. Importantly, all curves remain within the $\Lambda_{1,4}$ band determined by LIGO-Virgo. On the right panel, the plots show that, as the tidal deformability increases, the f -mode frequency decreases monotonically.

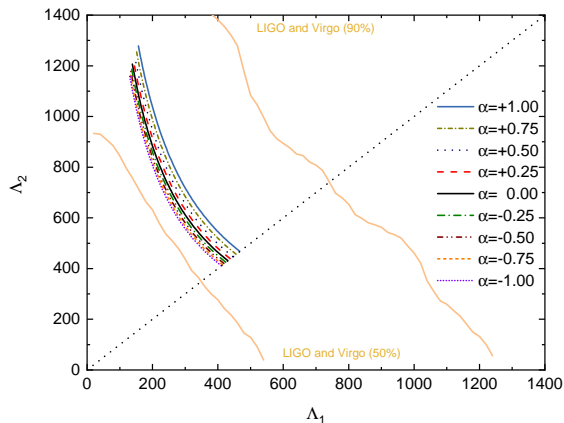


Figure 4. The dimensionless tidal deformabilities of the GW170817 event components are shown for different values of the anisotropic parameter α . The yellow line depicts the LIGO-Virgo confidence curves [1], while the dotted diagonal line marks the points where $\Lambda_1 = \Lambda_2$.

Using the observational data provided by LVC, the study in [1] established bounds on Λ_1 and Λ_2 , which quantify the dimensionless tidal deformability of the binary system. Here, Λ_1 corresponds to the tidal deformability of the more massive star, while Λ_2 refers to that of its companion. Fig. 4 presents the Λ_1 – Λ_2 plane, where each curve is generated by selecting a specific value of M_1 and then computing M_2 using the chirp mass $\mathcal{M} = 1.188 M_\odot$ [1], defined

as

$$\mathcal{M} = \frac{(M_1 M_2)^{3/5}}{(M_1 + M_2)^{1/5}}. \quad (4.5)$$

The stellar masses considered fall within the intervals $1.36 \leq M_1/M_\odot \leq 1.60$ and $1.17 \leq M_2/M_\odot \leq 1.36$, respectively. In addition, the 50% and 90% credibility contours for the GW170817 event, provided by LVC under the low-spin assumption, are included in the plot. For both $\alpha > 0$ and $\alpha < 0$, the effect of the anisotropy parameter on the tidal deformability becomes evident.

5 Conclusions

This article reports the effects of anisotropy on both the stellar structure and f oscillation modes of neutron stars. For this aim, we used the stellar equilibrium equations, including the anisotropic factor, and we derived the nonradial oscillation equations involving such a factor within the fully general relativity context. For the fluid contained in the star, we assume that the stellar matter obeys an equation of state derived from a consistent matching between microscopic nuclear theory and perturbative QCD calculations, joined through a piecewise polytropic interpolation scheme, and the anisotropy is described by the profile $\sigma = \alpha p_r (1 - \frac{1}{g_{11}})^2$ (see Ref. [33–35]).

Regarding the equilibrium configurations, we found that the neutron star is affected by anisotropy. For certain ranges of central energy density, we observed both higher (smaller) mass and radius values when using higher (lower) values of α . In addition, the change of α favors the proposed model, bringing the masses closer to the observational data. This suggests that anisotropy could play a relevant role in identifying neutron stars.

In our study of nonradial oscillation modes, we found that the f -modes are strongly influenced by anisotropy. For specific ranges of total mass, we observed that the f -modes increase (or decrease) as the anisotropy parameter α increases (or decreases). It is worth noting that the equations governing nonradial oscillations depend on the chosen anisotropic profile; in this case, they are determined by the form of equation (3.3).

We also investigated the impact of anisotropy on the detectability of the fundamental oscillation mode. Our results indicate that massive stars with an anisotropy parameter $\alpha \sim 1.0$ could be detected within our galaxy, i.e., at distances of approximately ~ 10 [kpc].

Finally, we also examine the consistency between the dimensionless tidal deformability of anisotropic neutron stars and the observational constraints reported by the LVC for the GW170817 event. Our analysis shows that the results presented in this work fall within the observational bounds provided by LVC. Our findings indicate that, when $\alpha > 0$, the tidal deformability decreases for larger values of α and, when $\alpha < 0$, the tidal deformability increases for lower values of α . Moreover, several studies in the literature have explored the tidal deformability of compact stars under various theoretical frameworks. For instance, [82] investigates this parameter considering quark matter in the color-flavor-locked phase of color superconductivity, [83] examines the role of isospin effects in strange quark matter, [84] analyzes the tidal deformability assuming a quasiparticle model that incorporates nonperturbative aspects of quantum chromodynamics in the low-density regime, and in [85] to constrain the nuclear matter equation of state from the neutron star tidal deformability. In all these works, as in the present study, constraints from the GW170817 event are used to place limits on the properties of compact stars within the corresponding theoretical scenarios.

Acknowledgments

The authors thank Shu Yan Lau, Siddarth Ajith, Victor Guedes, and Kent Yagi for useful discussions regarding the work. JDVA thanks Universidad Privada del Norte and Universidad Nacional Mayor de San Marcos for the financial support - RR No.005753-2021-R/UNMSM under the project number B21131781. JMZP acknowledges support from FAPERJ, Process SEI-260003/000308/2024. CVF acknowledges the financial support of the productivity program of the Conselho Nacional de Desenvolvimento Científico e Tecnológico (CNPq), with Project No. 304569/2022-4. CHL is thankful to the São Paulo Research Foundation FAPESP (Grant No. 2020/05238-9) and to CNPq (Grants No.401565/2023-8 and 305327/2023-2).

A Nonradial perturbations of relativistic spherically symmetric stars in the presence of an anisotropic fluid

A.1 Perturbative variables

For even-parity harmonics, the equations of motion are found through the perturbed Einstein's field equation (2.12), by employing the metric perturbation (2.16) and the Lagrangian fluid displacement vector components in the form

$$\xi^r = \frac{1}{r^2} e^{-\Lambda} W Y^{\ell m}, \quad (\text{A.1})$$

$$\xi^\theta = -\frac{1}{r^2} V \partial_\theta Y_{\ell m}, \quad (\text{A.2})$$

$$\xi^\phi = -\frac{1}{r^2 \sin^2 \theta} V \partial_\phi Y_{\ell m}, \quad (\text{A.3})$$

where W and V are functions be dependent on t and r . Moreover, the non-perturbed four-velocity and four-radial unit vectors are used, which are respectively placed as

$$u^{(0)\mu} = \left(\frac{1}{e^\Psi}, 0, 0, 0 \right) \quad \text{and} \quad k^{(0)\mu} = \left(0, \frac{1}{e^\Lambda}, 0, 0 \right), \quad (\text{A.4})$$

respectively. The perturbed four-velocity components are set in the form

$$\delta u^t = \frac{1}{2} \frac{H Y_{\ell m}}{e^\Psi}, \quad (\text{A.5})$$

$$\delta u^r = \frac{1}{e^\Psi} \frac{d\xi^r}{dr} = \frac{\dot{W} Y_{\ell m}}{r^2 e^{\Psi+\Lambda}}, \quad (\text{A.6})$$

$$\delta u^\theta = \frac{1}{e^\Psi} \frac{d\xi^\theta}{dr} = -\frac{\dot{V} \partial_\theta Y_{\ell m}}{r^2 e^\Psi}, \quad (\text{A.7})$$

$$\delta u^\phi = \frac{1}{e^\Psi} \frac{d\xi^\phi}{dr} = -\frac{\dot{V} \partial_\phi Y_{\ell m}}{r^2 e^\Psi \sin^2 \theta}, \quad (\text{A.8})$$

and the perturbed radial unit vectors given by

$$\delta k^0 = \frac{1}{e^\Psi} \left[\frac{H_1}{e^{\Psi+\Lambda}} + \frac{\dot{W}}{r^2 e^\Psi} \right] Y_{\ell m} \quad \text{and} \quad \delta k^1 = -\frac{1}{2} \frac{H}{e^\Lambda} Y_{\ell m}. \quad (\text{A.9})$$

The relations defined in Eqs. (A.4), (A.5), and (A.9) satisfy the equalities $g_{\mu\nu} k^\mu k^\nu = 1$, $g_{\mu\nu} u^\mu k^\nu = 0$, and $g_{\mu\nu} u^\mu u^\nu = 0$ in their both non-perturbed and perturbed form.

A.2 Perturbation equations

To obtain the equations of motion of the pulsating configuration, following Ref. [41], the Lagrangian perturbation of the baryon number density N is

$$\frac{\Delta N}{N} = \xi^k{}_{|k} - \frac{1}{2} \frac{\delta [{}^{(3)}g]}{{}^{(3)}g}. \quad (\text{A.10})$$

The term $\xi^k{}_{|k}$ denotes the covariant derivative in the 3-dimensional geometry at constant time, and the terms $\delta [{}^{(3)}g]$ and ${}^{(3)}g$ depict the determinant of the perturbed and unperturbed 3-dimensional metric, respectively. By employing the background metric (2.4), the metric perturbation (2.16), and the fluid displacement vectors (A.1)-(A.3), the equation (A.10) yields

$$\frac{\Delta N}{N} = -\frac{1}{2} H Y_{\ell m} - \frac{e^{-\Lambda}}{r^2} W' Y_{\ell m} - \frac{V}{r^2} \ell(\ell+1) Y_{\ell m} - K Y_{\ell m}. \quad (\text{A.11})$$

Using the baryon conservation equation, $\nabla_\mu (N u^\mu) = 0$, the local law of energy conservation ($u^\nu \nabla^\mu T_{\mu\nu} = 0$) in terms of Lagrangian perturbations yield (see [33]):

$$\Delta \rho = (\rho + p_r) \frac{\Delta N}{N} - \sigma \left(\Delta U_\theta^\theta + \Delta U_\phi^\phi \right), \quad (\text{A.12})$$

$$\Delta U_\theta^\theta + \Delta U_\phi^\phi = \left(K + 2e^{-\Lambda} \frac{W}{r^2} + \frac{\ell(\ell+1)}{r^2} V \right) Y_{\ell m}. \quad (\text{A.13})$$

Employing the relations of the thermodynamic functions in their Lagrangian and Eulerian forms, $\Delta \rho \approx \delta \rho + \frac{\partial \rho^0}{\partial r} \xi^r$, and equation (A.11), we find that equation (A.14) takes the form:

$$\begin{aligned} \delta \rho = & -(p_r + \rho) \left[\frac{H}{2} + \frac{e^{-\Lambda}}{r^2} W' + \frac{V}{r^2} \ell(\ell+1) + K \right] Y_{\ell m} - \sigma \left(K + \frac{V}{r^2} \ell(\ell+1) \right. \\ & \left. + \frac{2e^{-\Lambda}}{r^3} W \right) Y_{\ell m} - \rho' \frac{e^{-\Lambda}}{r^2} W Y_{\ell m}. \end{aligned} \quad (\text{A.14})$$

The perturbed radial pressure can be determined using the EOS $p_r = p_r(\rho)$, where $\delta p_r = \frac{dp_r}{d\rho} \delta\rho$. From Eq. (2.12), the nonnull perturbed Einstein field equations are given by

$$H' + \frac{He^{2\Lambda}}{r} \left[4\pi r^2(p_r - \rho) + 1 + \frac{\ell(\ell+1)}{2} \right] = rK'' - \frac{8\pi e^\Lambda W}{r} \left[\rho' + \frac{2\sigma}{r} \right] - \frac{8\pi e^{2\Lambda} V \ell(\ell+1)}{r} (p_r + \rho + \sigma) - \frac{8\pi e^\Lambda W'}{r} (p_r + \rho) - \frac{Ke^{2\Lambda}}{r} \left[8\pi r^2(p_r + \rho + \sigma) - 1 + \frac{\ell(\ell+1)}{2} \right] - e^{2\Lambda} \left[4\pi \rho r^2 + \frac{5m}{r} - 3 \right] K', \quad (\text{A.15})$$

$$\ell(\ell+1)H_1 = 2r^2\dot{K}' + 2r\dot{K}e^{2\Lambda} \left(-4\pi r^2 p_r - \frac{3m}{r} + 1 \right) - 2r\dot{H} - 16\pi(p_r + \rho)e^\Lambda \dot{W}, \quad (\text{A.16})$$

$$H_1' = -\frac{2e^\Lambda H_1}{r} \left[\frac{m}{r} + 2\pi r^2(p_r - \rho) \right] + e^{2\Lambda} \dot{H} + e^{2\Lambda} \dot{K} + 16\pi(\rho + p_r + \sigma)e^{2\Lambda} \dot{V}, \quad (\text{A.17})$$

$$\begin{aligned} & \ddot{K} - e^{2\Psi-2\Lambda} K'' - \frac{Ke^{2\Psi}}{r^2} \left(8\pi r^2 \left(\Gamma p_r - \rho - p_r - \sigma + \sigma \frac{dp_r}{d\rho} \right) - \ell(\ell+1) + 2 \right) \\ & - \frac{2K'e^{2\Psi}}{r} \left(1 - \frac{m}{r} + 2\pi r^2(p_r - \rho) \right) - \frac{e^{2\Psi} H}{r^2} \left(4\pi(p_r + \rho + \Gamma p_r)r^2 - 2 + \frac{4m}{r} \right) \\ & + \frac{W'e^{2\Psi-\Lambda}}{r^2} 8\pi(\rho + p_r - \Gamma p_r) + \frac{Ve^{2\Psi}}{r^2} 8\pi\ell(\ell+1) \left(\rho + p_r + \sigma - \Gamma p_r - \sigma \frac{dp_r}{d\rho} \right) \\ & + W \left(\rho' - p_r' + \frac{2\sigma}{r} \left(1 - \frac{dp_r}{d\rho} \right) \right) \frac{8\pi e^{2\Psi-\Lambda}}{r^2} = 0, \end{aligned} \quad (\text{A.18})$$

$$\dot{H}_1 = H'e^{2\Psi} - K'e^{2\Psi} + \frac{He^{2\Psi+2\Lambda}}{r} \left(\frac{2m}{r} + 8\pi r^2 p_r \right). \quad (\text{A.19})$$

From the perturbed conservation law of the energy-momentum tensor components $\delta(\nabla_\nu T_1^\nu)$ and $\delta(\nabla_\nu T_2^\nu)$, we respectively obtain:

$$\begin{aligned} & -\frac{H'}{2}(p_r + \rho)e^\Psi - e^\Psi \Psi'(p_r + \rho) \left[\frac{H}{2} + \frac{V}{r^2} \ell(\ell+1) + K \right] - e^\Psi \Psi' \sigma \left[\frac{2e^{-\Lambda}}{r^3} W \right. \\ & + \frac{V}{r^2} \ell(\ell+1) + K \left. \right] - \left\{ e^\Psi (p_r + \rho) \frac{dp_r}{d\rho} \left[\frac{H}{2} + \frac{e^{-\Lambda}}{r^2} W' + \frac{V}{r^2} \ell(\ell+1) + K \right] \right. \\ & \left. + e^\Psi \sigma \frac{dp_r}{d\rho} \left(K + \frac{\ell(\ell+1)V}{r^2} + \frac{2e^{-\Lambda}W}{r^3} \right) \right\}' - K' \sigma e^\Psi + (p_r + \rho) \frac{e^{\Lambda-\Psi}}{r^2} \ddot{W} \\ & + (p_r + \rho) e^\Psi \left[H' - K' + \frac{H}{r} e^{2\Lambda} \left(\frac{2m}{r} + 8\pi r^2 p_r \right) \right] + (p_r + \rho) (\Psi'^2 + \Psi'' - \Psi' \Lambda') \\ & - \frac{2\Psi'}{r} \frac{e^{\Psi-\Lambda}}{r^2} W - \frac{2}{r^3} \left(\frac{3\sigma}{r} - \sigma' - \sigma \left(\frac{2me^{2\Lambda}}{r^2} + 4\pi e^{2\Lambda} (p_r - \rho)r \right) \right) e^{\Psi-\Lambda} W - \frac{2\sigma}{r^3} e^{\Psi-\Lambda} W' \\ & + p_r' \Psi' \frac{e^{\Psi-\Lambda}}{r^2} W - \frac{2e^\Psi}{r} (\delta\tilde{\sigma}) = 0, \end{aligned} \quad (\text{A.20})$$

$$\begin{aligned} & (p_r + \rho + \sigma) \frac{\ddot{V}}{e^{2\Psi}} + \frac{H}{2} (p_r + \rho + \Gamma p_r) + \frac{W'}{r^2 e^\Lambda} \Gamma p_r + \frac{V\ell(\ell+1)}{r^2} (\Gamma p_r \\ & + \sigma \frac{dp_r}{d\rho}) + K \left(\Gamma p_r + \sigma \frac{dp_r}{d\rho} \right) + W \left(\frac{p_r'}{r^2 e^\Lambda} + \frac{2\sigma}{e^\Lambda r^3} \frac{dp_r}{d\rho} \right) - \delta\tilde{\sigma} = 0, \end{aligned} \quad (\text{A.21})$$

where $\Gamma = (p_r + \rho) \frac{dp_r}{d\rho}$ and $\delta\sigma = \delta\tilde{\sigma} Y_{\ell m}$. It is important to mention that the term $\delta\tilde{\sigma}$ is renamed as $\delta\sigma$. In addition, for the anisotropic profile $\sigma = \sigma(p_r, g_{11})$, we found that

$$\delta\sigma = \frac{\partial\sigma}{\partial p_r} \delta p_r + \frac{\partial\sigma}{\partial g_{11}} h_{11}. \quad (\text{A.22})$$

This last relation is also used to determine Eqs. (2.17)-(2.22). It is important to mention that, in the Cowling approximation, $h_{\mu\nu}=0$, Eqs. (A.14)-(A.22) reproduce the nonradial oscillation equations reported in Ref. [45].

B Perturbation functions near $r = 0$

For the isotropic case, $\sigma = 0$, the spacetime perturbation and fluid functions expanded in a power series near $r = 0$ have been previously reported in Ref. [43]. This appendix shows these expanded functions for the anisotropic case, $\sigma \neq 0$. Since we seek solutions to the perturbation equations (2.18)-(2.21), the perturbation functions $\tilde{H}_1(r)$, $\tilde{K}(r)$, $\tilde{W}(r)$, and $\tilde{X}(r)$ near the center of the star are considered into the form

$$\tilde{H}_1(r) = \tilde{H}_1(0) + \frac{1}{2} \tilde{H}_1''(0) r^2 + O(r^4), \quad (\text{B.1})$$

$$\tilde{K}(r) = \tilde{K}(0) + \frac{1}{2} \tilde{K}''(0) r^2 + O(r^4), \quad (\text{B.2})$$

$$\tilde{W}(r) = \tilde{W}(0) + \frac{1}{2} \tilde{W}''(0) r^2 + O(r^4), \quad (\text{B.3})$$

$$\tilde{X}(r) = \tilde{X}(0) + \frac{1}{2} \tilde{X}''(0) r^2 + O(r^4), \quad (\text{B.4})$$

where the first-order $-\tilde{H}_1(0)$, $\tilde{K}(0)$, $\tilde{W}(0)$, and $\tilde{X}(0)$ - and second-order coefficients $-\tilde{H}_1''(0)$, $\tilde{K}''(0)$, $\tilde{W}''(0)$, and $\tilde{X}''(0)$ - are constants. The first-order terms are given by:

$$\tilde{H}(0) = \tilde{K}(0), \quad (\text{B.5})$$

$$\tilde{X}(0) = (\rho_0 + p_{r0}) e^{\Psi_0} \left[-\frac{\omega^2 e^{-2\Psi_0}}{\ell} \tilde{W}(0) + \frac{4\pi}{3} (\rho_0 + 3p_{r0}) \tilde{W}(0) - \frac{\tilde{K}(0)}{2} \right], \quad (\text{B.6})$$

$$\tilde{H}_1(0) = \left[\frac{2\ell \tilde{K}(0) - 16\pi(\rho_0 + p_{r0}) \tilde{W}(0)}{\ell(\ell + 1)} \right], \quad (\text{B.7})$$

$$\tilde{V}(0) = -\frac{1}{\ell} \tilde{W}(0), \quad (\text{B.8})$$

with the constants ρ_0 , p_{r0} , and Ψ_0 representing the first-order terms of the power-series expansions:

$$\rho(r) = \rho_0 + \frac{1}{2} \rho_2 r^2, \quad (\text{B.9})$$

$$p_r(r) = p_{r0} + \frac{1}{2} p_{r2} r^2 + \frac{1}{4} p_{r4} r^4, \quad (\text{B.10})$$

$$\Psi(r) = \Psi_0 + \frac{1}{2} \Psi_2 r^2 + \frac{1}{4} \Psi_4 r^4, \quad (\text{B.11})$$

$$\sigma(r) = \sigma_0 + \frac{1}{2} \sigma_2 r^2 + \frac{1}{4} \sigma_4 r^4, \quad (\text{B.12})$$

and α being the dimensionless anisotropic constant. Through equation (3.3), we can see that in the star's center, because $g_{11} = 1$ (see Eq. (2.8)), we have $\sigma_0 = 0$. The second and fourth-order coefficients of the power-series (B.9)-(B.12) are

$$\Psi_2 = \frac{4\pi}{3}(\rho_0 + 3p_{r0}), \quad (\text{B.13})$$

$$\rho_2 = -\frac{(\rho_0 + p_{r0})^2}{\Gamma p_{r0}}\Psi_2, \quad (\text{B.14})$$

$$\sigma_2 = 0, \quad (\text{B.15})$$

$$p_{r2} = -(\rho_0 + p_{r0})\Psi_2, \quad (\text{B.16})$$

$$\Psi_4 = \frac{2\pi}{5}(\rho_2 + 5p_{r2}) + \frac{32\pi^2}{9}\rho_0(\rho_0 + 3p_{r0}), \quad (\text{B.17})$$

$$\sigma_4 = \left(\frac{16\pi\rho_0}{3}\right)^2 p_{r0}\alpha, \quad (\text{B.18})$$

$$p_{r4} = -(p_{r0} + \rho_0)\Psi_4 - \frac{1}{2}(p_{r2} + \rho_2)\Psi_2 + \frac{1}{2}\sigma_4. \quad (\text{B.19})$$

Note that all coefficients shown in Eqs. (B.13)-(B.19) are concord with those obtained for the isotropic case. Since when $\alpha = 0$, Eqs. (B.13)-(B.17) and (B.19) reproduce the equalities reported in Ref. [19] and with the equalities (B.15) and (B.18) being identically null. Moreover, by evaluating the perturbation equation to the second-order terms $[\tilde{H}_1''(0), \tilde{K}''(0), \tilde{W}''(0), \tilde{X}''(0)]$, we find that the following relationships must hold:

$$\begin{aligned} \frac{\ell+3}{2}\tilde{H}_1''(0) - \tilde{K}''(0) + 8\pi(p_{r0} + \rho_0)\frac{\ell+3}{\ell(\ell+1)}\tilde{W}''(0) &= 4\pi\left[\frac{1}{3}(2\ell+3)\rho_0 - p_{r0}\right]\tilde{H}_1(0) \\ + 8\pi(p_{r0} + \rho_0)Q_1 + \frac{1}{2}Q_0 - \frac{8\pi}{\ell}(p_{r2} + \rho_2)\tilde{W}(0), \end{aligned} \quad (\text{B.20})$$

$$\begin{aligned} \frac{\ell+2}{2}\tilde{K}''(0) - \frac{\ell(\ell+1)}{4}\tilde{H}_1''(0) - 4\pi(p_{r0} + \rho_0)\tilde{W}''(0) &= 4\pi\left[p_{r2} + \rho_2 + \frac{8\pi}{3}\rho_0(p_{r0} + \rho_0)\right]\tilde{W}(0) \\ + \frac{1}{2}Q_0 + \left(\frac{4\pi}{3}\rho_0 + 4\pi p_{r0}\right)\tilde{K}(0), \end{aligned} \quad (\text{B.21})$$

$$\begin{aligned} \frac{\ell+2}{2}\tilde{X}''(0) + \frac{\ell(\ell+1)}{8}e^{\Psi_0}(p_{r0} + \rho_0)\tilde{H}_1''(0) + e^{\Psi_0}(p_{r0} + \rho_0) &\left[\frac{\omega^2}{2}e^{-2\Psi_0} + 2\pi(p_{r0} + \rho_0)\right. \\ \left. - \frac{\ell+2}{2}\Psi_2\right]\tilde{W}''(0) &= \frac{\ell}{2}\left(\Psi_2 + \frac{p_{r2} + \rho_2}{p_{r0} + \rho_0}\right)\tilde{X}(0) + e^{\Psi_0}(p_{r0} + \rho_0)\left[-\frac{\ell(\ell+1)}{2}\Psi_2 Q_1 - \frac{1}{4}Q_0\right. \\ \left. - \left(\frac{\omega^2}{2}e^{-2\Psi_0}\right)\tilde{H}_1(0) - \Psi_2\tilde{K}(0) + \left\{(\ell+2)\Psi_4 - 2\pi(p_{r2} + \rho_2) - \frac{16\pi^2}{3}\rho_0(p_{r0} + \rho_0) - \frac{4\pi}{3}\rho_0\Psi_2\right. \right. \\ \left. \left. + \omega^2e^{-2\Psi_0}\left(\Psi_2 - \frac{4\pi}{3}\rho_0\right) - \frac{\sigma_4}{p_{r0} + \rho_0}\right\}\tilde{W}(0)\right], \end{aligned} \quad (\text{B.22})$$

$$\begin{aligned} -\frac{1}{4}(p_{r0} + \rho_0)\tilde{K}''(0) - \frac{1}{2}\left[p_{r2} + \frac{\ell+3}{\ell(\ell+1)}\omega^2e^{-2\Psi_0}(p_{r0} + \rho_0)\right]\tilde{W}''(0) &- \frac{1}{2}e^{-\Psi_0}\tilde{X}''(0) \\ = -\frac{1}{2}e^{-\Psi_0}\Psi_2\tilde{X}(0) + \frac{1}{4}(p_{r2} + \rho_2)\tilde{K}(0) + \frac{1}{4}(p_{r0} + \rho_0)Q_0 &+ \left[\frac{\omega^2}{\ell}e^{-2\Psi_0}\left[\frac{1}{2}(p_{r2} + \rho_2)\right.\right. \\ \left. \left. - (p_{r0} + \rho_0)\Psi_2\right] + p_{r4} - \frac{4\pi}{3}\rho_0 p_{r2}\right]\tilde{W}(0) &- \frac{1}{2}\omega^2e^{-2\Psi_0}(p_{r0} + \rho_0)Q_1, \end{aligned} \quad (\text{B.23})$$

with Q_0 and Q_1 defined by

$$Q_0 = \frac{4}{(\ell+2)(\ell-1)} \left[-8\pi e^{-\Psi_0} \tilde{X}(0) - \left(\omega^2 e^{-2\Psi_0} + \frac{8\pi}{3} \rho_0 \right) \tilde{K}(0) + \left[\omega^2 e^{-2\Psi_0} - \ell(\ell+1) \left(\frac{2\pi}{3} \rho_0 + 2\pi p_{r_0} \right) \right] \tilde{H}_1(0) \right], \quad (\text{B.24})$$

$$Q_1 = \frac{2}{\ell(\ell+1)} \left[\frac{4\pi}{3} (\ell+1) \rho_0 \tilde{W}(0) - \frac{3}{2} \tilde{K}(0) + \frac{e^{-\Psi_0}}{\Gamma p_{r_0}} \tilde{X}(0) \right]. \quad (\text{B.25})$$

It is important to mention that all equations presented in this section agree with those presented in [19, 43] for the isotropic case. In addition, the expansion of Eq. (B.21) to the leading order is the same as Eq. (B.6).

References

- [1] B.P. Abbott and et al., *GW170817: Observation of Gravitational Waves from a Binary Neutron Star Inspiral*, *Phys. Rev. Lett.* **119** (2017) 161101 [[1710.05832](#)].
- [2] B.P. Abbott and et al., *Observation of Gravitational Waves from a Binary Black Hole Merger*, *Phys. Rev. Lett.* **116** (2016) 061102 [[1602.03837](#)].
- [3] B.P. Abbott and et al., *GW151226: Observation of Gravitational Waves from a 22-Solar-Mass Binary Black Hole Coalescence*, *Phys. Rev. Lett.* **116** (2016) 241103 [[1606.04855](#)].
- [4] B.P. Abbott and et al., *Tests of General Relativity with GW150914*, *Phys. Rev. Lett.* **116** (2016) 221101 [[1602.03841](#)].
- [5] B.P. Abbott and et al., *GW170104: Observation of a 50-Solar-Mass Binary Black Hole Coalescence at Redshift 0.2*, *Phys. Rev. Lett.* **118** (2017) 221101 [[1706.01812](#)].
- [6] B.P. Abbott and et al., *GW170814: A Three-Detector Observation of Gravitational Waves from a Binary Black Hole Coalescence*, *Phys. Rev. Lett.* **119** (2017) 141101 [[1709.09660](#)].
- [7] B.P. Abbott and et al., *GW170608: Observation of a 19 Solar-mass Binary Black Hole Coalescence*, *Astrophys. J. Lett.* **851** (2017) L35 [[1711.05578](#)].
- [8] B.P. Abbott and et al., *Astrophysical Implications of the Binary Black-hole Merger GW150914*, *Astrophys. J. Lett.* **818** (2016) L22 [[1602.03846](#)].
- [9] B.P. Abbott and et al., *Multi-messenger Observations of a Binary Neutron Star Merger*, *Astrophys. J. Lett.* **848** (2017) L12 [[1710.05833](#)].
- [10] A.L. Miller and F. De Lillo, *Searching for continuous gravitational waves from highly deformed compact objects with decigo*, *Phys. Rev. D* **112** (2025) 042001.
- [11] G. Miniutti, J.A. Pons, E. Berti, L. Gualtieri and V. Ferrari, *Non-radial oscillation modes as a probe of density discontinuities in neutron stars*, *Mon. Not. R. Astron. Soc.* **338** (2003) 389 [[astro-ph/0206142](#)].
- [12] A. Passamonti, M. Bruni, L. Gualtieri, A. Nagar and C.F. Sopuerta, *Coupling of radial and axial nonradial oscillations of compact stars: Gravitational waves from first-order differential rotation*, *Phys. Rev. D* **73** (2006) 084010 [[gr-qc/0601001](#)].
- [13] G.J. Savonije, *Non-radial oscillations of the rapidly rotating Be star HD 163868*, *Astro. Astrop.* **469** (2007) 1057 [[0705.1755](#)].
- [14] C.V. Flores, Z.B. Hall and P. Jaikumar, *Nonradial oscillation modes of compact stars with a crust*, *Phys. Rev. C* **96** (2017) 065803 [[1708.05985](#)].

- [15] H. Sotani and T. Harada, *Nonradial oscillations of quark stars*, *Phys. Rev. D* **68** (2003) 024019 [[gr-qc/0307035](#)].
- [16] C.V. Flores and G. Lugones, *Constraining color flavor locked strange stars in the gravitational wave era*, *Phys. Rev. C* **95** (2017) 025808 [[1702.02081](#)].
- [17] N. Andersson and K.D. Kokkotas, *Towards gravitational wave asteroseismology*, *Mon. Not. R. Astron. Soc.* **299** (1998) 1059 [[gr-qc/9711088](#)].
- [18] O. Benhar, V. Ferrari and L. Gualtieri, *Gravitational wave asteroseismology reexamined*, *Phys. Rev. D* **70** (2004) 124015 [[astro-ph/0407529](#)].
- [19] H. Sotani, K. Tominaga and K.-I. Maeda, *Density discontinuity of a neutron star and gravitational waves*, *Phys. Rev. D* **65** (2001) 024010 [[gr-qc/0108060](#)].
- [20] C.V. Flores, C.H. Lenzi, M. Dutra, O. Lourenço and J.D.V. Arbañil, *Gravitational wave asteroseismology of dark matter hadronic stars*, *Phys. Rev. D* **109** (2024) 083021 [[2402.12600](#)].
- [21] F. Gittins, N. Andersson and D.I. Jones, *Modelling neutron star mountains*, *MNRAS* **500** (2020) 5570.
- [22] F. Gittins and N. Andersson, *Modelling neutron star mountains in relativity*, *MNRAS* **507** (2021) 116.
- [23] P. Pnigouras, N. Andersson, F. Gittins and A.R. Counsell, *Dynamical neutron-star tides: The signature of a mode resonance*, *MNRAS* (2025) [staf1285](#).
- [24] A.I. Sokolov, *Phase transitions in a superfluid neutron liquid*, *Soviet Journal of Experimental and Theoretical Physics* **52** (1980) 575.
- [25] B. Carter and D. Langlois, *Relativistic models for superconducting-superfluid mixtures*, *Nucl. Phys. B* **531** (1998) 478.
- [26] S.S. Yazadjiev, *Relativistic models of magnetars: Nonperturbative analytical approach*, *Phys. Rev. D* **85** (2012) 044030.
- [27] L. Herrera and N. Santos, *Local anisotropy in self-gravitating systems*, *Phys. Rep.* **286** (1997) 53.
- [28] J. Kumar and P. Bharti, *Relativistic models for anisotropic compact stars: A review*, *New Astron. Rev.* **95** (2022) 101662.
- [29] E.J.A. Curi, L.B. Castro, C.V. Flores and C.H. Lenzi, *Non-radial oscillations and global stellar properties of anisotropic compact stars using realistic equations of state*, *Eur. Phys. J. C* **82** (2022) 527.
- [30] H.C. Das and L.L. Lopes, *Anisotropic strange stars in the spotlight: unveiling constraints through observational data*, *MNRAS* **525** (2023) 3571.
- [31] J.M.Z. Pretel, T. Tangphati, A. Banerjee and A. Pradhan, *Effects of anisotropic pressure on interacting quark star structure*, *Phys. Lett. B* **848** (2024) 138375.
- [32] L.M. Becerra, E.A. Becerra-Vergara and F.D. Lora-Clavijo, *Realistic anisotropic neutron stars: Pressure effects*, *Phys. Rev. D* **109** (2024) 043025.
- [33] S.Y. Lau, S. Ajith, V. Guedes and K. Yagi, *Nonradial instabilities in anisotropic neutron stars*, *Phys. Rev. D* **110** (2024) 083020 [[2405.04653](#)].
- [34] J. Yu, V. Guedes, S.Y. Lau, S. Ajith and K. Yagi, *Spacetime Quasi-normal Mode Oscillations of Anisotropic Neutron Stars*, *arXiv e-prints* (2026) [arXiv:2601.06962](#) [[2601.06962](#)].
- [35] V. Guedes, S. Ajith, S.Y. Lau and K. Yagi, *Gravitational-wave constraints on neutron-star pressure anisotropy via universal relations*, *Phys. Rev. D* **113** (2026) 043025 [[2510.26042](#)].
- [36] S. Mondal and M. Bagchi, *f-mode oscillations of anisotropic neutron stars in full general relativity*, *Phys. Rev. D* **110** (2024) 123011 [[2309.00439](#)].

- [37] S. Mondal and M. Bagchi, *Quasinormal f-modes of anisotropic quark stars in full general relativity*, *Phys. Rev. D* **111** (2025) 103035 [2504.20589].
- [38] R.C. Tolman, *Static Solutions of Einstein's Field Equations for Spheres of Fluid*, *Physical Review* **55** (1939) 364.
- [39] J.R. Oppenheimer and G.M. Volkoff, *On Massive Neutron Cores*, *Physical Review* **55** (1939) 374.
- [40] R.L. Bowers and E.P.T. Liang, *Anisotropic Spheres in General Relativity*, *Astrophys. J.* **188** (1974) 657.
- [41] K.S. Thorne and A. Campolattaro, *Non-Radial Pulsation of General-Relativistic Stellar Models. I. Analytic Analysis for $L \geq 2$* , Sept., 1967. 10.1086/149288.
- [42] T. Regge and J.A. Wheeler, *Stability of a Schwarzschild Singularity*, *Physical Review* **108** (1957) 1063.
- [43] L. Lindblom and S.L. Detweiler, *The quadrupole oscillations of neutron stars.*, *Astrophys. J. Suppl. Ser.* **53** (1983) 73.
- [44] S. Detweiler and L. Lindblom, *On the nonradial pulsations of general relativistic stellar models*, *Astrophys. J.* **292** (1985) 12.
- [45] D.D. Doneva and S.S. Yazadjiev, *Nonradial oscillations of anisotropic neutron stars in the Cowling approximation*, *Phys. Rev. D* **85** (2012) 124023 [1203.3963].
- [46] J.D.V. Arbañil, C.V. Flores, C.H. Lenzi and J.M.Z. Pretel, *Fluid pulsation modes and tidal deformability of anisotropic strange stars in light of the GW170817 event*, *Phys. Rev. D* **107** (2023) 124016 [2305.13468].
- [47] J.-L. Lü and W.-M. Suen, *Determining the long living quasi-normal modes of relativistic stars*, *Chinese Physics B* **20** (2011) 040401.
- [48] F.J. Zerilli, *Effective Potential for Even-Parity Regge-Wheeler Gravitational Perturbation Equations*, *Phys. Rev. Lett.* **24** (1970) 737.
- [49] E.D. Fackerell, *Solutions of Zerilli's Equation for Even-Parity Gravitational Perturbations*, *Astrophys. J.* **166** (1971) 197.
- [50] S. Chandrasekhar and S. Detweiler, *The Quasi-Normal Modes of the Schwarzschild Black Hole*, *Proceedings of the Royal Society of London Series A* **344** (1975) 441.
- [51] A. Akmal, V.R. Pandharipande and D.G. Ravenhall, *Equation of state of nucleon matter and neutron star structure*, *Phys. Rev. C* **58** (1998) 1804.
- [52] L. Coraggio, J.W. Holt, N. Itaco, R. Machleidt and F. Sammarruca, *Reduced regulator dependence of neutron-matter predictions with perturbative chiral interactions*, *Phys. Rev. C* **87** (2013) 014322 [1209.5537].
- [53] S. Gandolfi, J. Carlson and S. Reddy, *Maximum mass and radius of neutron stars, and the nuclear symmetry energy*, *Phys. Rev. C* **85** (2012) 032801.
- [54] J.W. Holt, N. Kaiser and W. Weise, *Chiral fermi liquid approach to neutron matter*, *Phys. Rev. C* **87** (2013) 014338.
- [55] K. Hebeler and A. Schwenk, *Chiral three-nucleon forces and neutron matter*, *Phys. Rev. C* **82** (2010) 014314.
- [56] F. Sammarruca, B. Chen, L. Coraggio, N. Itaco and R. Machleidt, *Dirac-brueckner-hartree-fock versus chiral effective field theory*, *Phys. Rev. C* **86** (2012) 054317.
- [57] I. Tews, T. Krüger, K. Hebeler and A. Schwenk, *Neutron matter at next-to-next-to-next-to-leading order in chiral effective field theory*, *Phys. Rev. Lett.* **110** (2013) 032504.

- [58] A. Kurkela, E.S. Fraga, J. Schaffner-Bielich and A. Vuorinen, *Constraining neutron star matter with quantum chromodynamics*, *The Astrophysical Journal* **789** (2014) 127.
- [59] A. Kurkela, P. Romatschke and A. Vuorinen, *Cold quark matter*, *Phys. Rev. D* **81** (2010) 105021.
- [60] E.S. Fraga, A. Kurkela and A. Vuorinen, *Interacting quark matter equation of state for compact stars*, *The Astrophysical Journal Letters* **781** (2014) L25.
- [61] I. Tews, T. Krüger, K. Hebeler and A. Schwenk, *Neutron matter at next-to-next-to-next-to-leading order in chiral effective field theory*, *Phys. Rev. Lett.* **110** (2013) 032504 [1206.0025].
- [62] P.B. Demorest, T. Pennucci, S.M. Ransom, M.S.E. Roberts and J.W.T. Hessels, *A two-solar-mass neutron star measured using Shapiro delay*, *Nature* **467** (2010) 1081 [1010.5788].
- [63] J. Antoniadis and et al., *A Massive Pulsar in a Compact Relativistic Binary*, *Science* **340** (2013) 448 [1304.6875].
- [64] D. Horvat, S. Ilijić and A. Marunović, *Radial pulsations and stability of anisotropic stars with a quasi-local equation of state*, *Classical and Quantum Gravity* **28** (2011) 025009 [1010.0878].
- [65] J.D.V. Arbañil and G. Panotopoulos, *Tidal deformability and radial oscillations of anisotropic polytropic spheres*, *Phys. Rev. D* **105** (2022) 024008 [2112.09729].
- [66] J.D.V. Arbañil and M. Malheiro, *Radial stability of anisotropic strange quark stars*, *J. Cosmol. Astropart. Phys.* **2016** (2016) 012 [1607.03984].
- [67] V. Folomeev and V. Dzhunushaliev, *Magnetic fields in anisotropic relativistic stars*, *Phys. Rev. D* **91** (2015) 044040 [1501.06275].
- [68] H.O. Silva, C.F.B. Macedo, E. Berti and L.C.B. Crispino, *Slowly rotating anisotropic neutron stars in general relativity and scalar-tensor theory*, *Classical and Quantum Gravity* **32** (2015) 145008 [1411.6286].
- [69] J.M.Z. Pretel, *Moment of inertia of slowly rotating anisotropic neutron stars in $f(R,T)$ gravity*, *Modern Physics Letters A* **37** (2022) 2250188 [2301.02881].
- [70] J.-L. Lü and W.-M. Suen, *Determining the long living quasi-normal modes of relativistic stars*, *Chinese Physics B* **20** (2011) 040401.
- [71] C. Vásquez Flores and G. Lugones, *Discriminating hadronic and quark stars through gravitational waves of fluid pulsation modes*, *Classical and Quantum Gravity* **31** (2014) 155002 [1310.0554].
- [72] T.E. Riley and et al., *A NICER View of PSR J0030+0451: Millisecond Pulsar Parameter Estimation*, *Astrophys. J. Lett.* **887** (2019) L21 [1912.05702].
- [73] M.C. Miller and et al., *PSR J0030+0451 Mass and Radius from NICER Data and Implications for the Properties of Neutron Star Matter*, *Astrophys. J. Lett.* **887** (2019) L24 [1912.05705].
- [74] T.E. Riley and et al., *A NICER View of the Massive Pulsar PSR J0740+6620 Informed by Radio Timing and XMM-Newton Spectroscopy*, *Astrophys. J. Lett.* **918** (2021) L27 [2105.06980].
- [75] M.C. Miller and et al., *The Radius of PSR J0740+6620 from NICER and XMM-Newton Data*, *Astrophys. J. Lett.* **918** (2021) L28 [2105.06979].
- [76] H.T. Cromartie and et al., *Relativistic Shapiro delay measurements of an extremely massive millisecond pulsar*, *Nature Astronomy* **4** (2020) 72 [1904.06759].
- [77] J. Powell and P.D. Lasky, *The dawes review 12: Gravitational-wave burst astrophysics*, *Publications of the Astronomical Society of Australia* **42** (2025) e030.

- [78] K.D. Kokkotas, T.A. Apostolatos and N. Andersson, *The inverse problem for pulsating neutron stars: a ‘fingerprint analysis’ for the supranuclear equation of state*, *Monthly Notices of the Royal Astronomical Society* **320** (2001) 307 [<https://academic.oup.com/mnras/article-pdf/320/3/307/3793761/320-3-307.pdf>].
- [79] F. Echeverria, *Gravitational-wave measurements of the mass and angular momentum of a black hole*, *Phys. Rev. D* **40** (1989) 3194.
- [80] B.P. Abbott, R. Abbott, T.D. Abbott, M.R. Abernathy, K. Ackley, C. Adams et al., *Exploring the sensitivity of next generation gravitational wave detectors*, *Classical and Quantum Gravity* **34** (2017) 044001 [[1607.08697](https://arxiv.org/abs/1607.08697)].
- [81] B.P. Abbott, R. Abbott, T.D. Abbott, F. Acernese, K. Ackley, C. Adams et al., *GW170817: Measurements of Neutron Star Radii and Equation of State*, *Phys. Rev. Lett.* **121** (2018) 161101 [[1805.11581](https://arxiv.org/abs/1805.11581)].
- [82] O. Lourenço, C.H. Lenzi, M. Dutra, E.J. Ferrer, V.d.l. Incera, L. Paulucci et al., *Tidal deformability of strange stars and the gw170817 event*, *Phys. Rev. D* **103** (2021) 103010 [[2104.07825](https://arxiv.org/abs/2104.07825)].
- [83] B.-L. Li, Y. Yan and J.-L. Ping, *Tidal deformabilities and radii of strange quark stars*, *Phys. Rev. D* **104** (2021) 043002.
- [84] J.-F. Xu, C.-J. Xia, Z.-Y. Lu, G.-X. Peng and Y.-P. Zhao, *Symmetry energy of strange quark matter and tidal deformability of strange quark stars*, *Nuclear Science and Techniques* **33** (2022) 143.
- [85] T. Malik, N. Alam, M. Fortin, C. Providência, B.K. Agrawal, T.K. Jha et al., *GW170817: Constraining the nuclear matter equation of state from the neutron star tidal deformability*, *Phys. Rev. C* **98** (2018) 035804 [[1805.11963](https://arxiv.org/abs/1805.11963)].